Chemical inhomogeneity in the near-surface region of $KTaO_3$ evolving at elevated temperatures

2000 J. Phys.: Condens. Matter 12 4687

(http://iopscience.iop.org/0953-8984/12/22/302)

J. Phys.: Condens. Matter **12** (2000) 4687–4697. Printed in the UK PII: S0953-8984(00)05797-0

Chemical inhomogeneity in the near-surface region of $KTaO_3$ evolving at elevated temperatures

K Szot†[#], W Speier‡, M Pawelczyk§, J Kwapuliñski§, J Hulliger‖, H Hesse¶, U Breuer[+] and W Quadakkers[*]

† Institute für Festkörperforschung, Forschungszentrum Jülich GmbH, D 52425 Jülich, Germany
‡ Institut für Chemie und Dynamik der Geosphäre, Forschungszentrum Jülich GmbH, D 52425 Jülich, Germany
§ Institute of Physics, Silesian University, PL 40-007 Katowice, Poland
‖ Departement für Chemie und Biochemie, Universität Bern, Freiestraße 3, CH-3012 Bern, Switzerland
¶ Fachbereich Physik, Universität Osnabrück, Barbarastraße 7, D-49069 Osnabrück, Germany
[+] Zentralabteilung für Chemische Analysen, Forschungszentrum Jülich GmbH, D 52425 Jülich, Germany
[*] Institut für Werkstoffe und Verfahren der Energietechnik, Forschungszentrum Jülich GmbH, D 52425 Jülich, Germany

Received 7 June 1999

Abstract. Measurements by x-ray diffraction, secondary ion mass spectrometry and atomic force microscopy are reported for single crystalline $KTaO_3$ after thermal treatment under oxidizing conditions in the temperature range of 700 to 1100 °C. The formation of a series of new phases $KO^*(KTaO_3)_n$ of Ruddlesden–Popper type is observed. Atomic force microscopy of (100) surfaces reveals corresponding dramatic changes in the surface morphology. Secondary ion mass spectrometry gives evidence of a redistribution of material leading to an enrichment of K with respect to Ta close to the surface and a corresponding depletion in deeper parts of the near-surface region. The results are in strong contrast to standard point defect models. Instead, our experimental observations have to be interpreted in terms of an evolving chemical inhomogeneity due to segregation processes in the near-surface region of the crystals and intergrowth of KO, which results in the formation of the Ruddlesden–Popper phases. The additional effect of K_2O evaporation above 900 °C is discussed and the corresponding topographical changes induced are documented.

$KTaO_3$ can be regarded as a prototype perovskite of ABO_3 structure. It retains the cubic structure down to the lowest temperatures and remains paraelectric. Together with $SrTiO_3$, the ground state of $KTaO_3$ serves as an example case for the electronic structure of the ABO_3 perovskites. Correspondingly, the electronic structure has been calculated by various bandstructure schemes since the early 70s [1], which have all established the insulating character of $KTaO_3$ and have successfully described available photoelectron and optical spectra (see, e.g., [2]). Moreover, the absence of ferroelectricity has been confirmed theoretically [3]. This material is also of technological interest as a substrate for pyrodetectors [4] and high T_c superconductors [5] or as potential material for microelectronics.

Introduction of defects in $KTaO_3$ has several important effects. For instance, ferroelectric behaviour can be induced by a very low level of doping [6]. Concerning the electrical properties,

[#] Permanent address: Institute of Physics, Silesian University, PL 40-007 Katowice, Poland.

0953-8984/00/224687+11$30.00

chemical doping leads to the introduction of electrons or holes and generates semiconducting behaviour. The same holds true for thermal treatment of the pure material which is why this is also sometimes termed 'self-doping'. The corresponding defect chemistry diagram for reduced and oxidized $KTaO_3$ has been determined for temperatures above 900 °C [7] and interpreted within the standard defect model of a statistical distribution of point defects (see also a recent theoretical analysis by [8, 9]). However, the comparison with its close relative, $KNbO_3$, poses a few intriguing questions. First of all, the electrical measurements for the defect chemistry diagram are conducted at relatively high temperatures. Yet, it is well known for $KNbO_3$ that such temperatures cause a dramatic loss of alkali metal oxides ([10], see also [11], and references therein). Second, segregation effects are observed in $KNbO_3$ at elevated temperatures which lead to the formation of chemical phases of Ruddlesden–Popper (RP) type in the near-surface region [12]. And finally, also the surface morphology of $KNbO_3$ seems to be drastically altered as a consequence of thermal treatment [12].

These issues bring into focus the effects of heat treatment on the surface and near-surface region of $KTaO_3$ for temperatures which are not generally considered as controversial for this material. Single crystals of $KTaO_3$ also offer the possibility to study the effect of thermal treatment without being hampered by a ferroelectric domain structure and phase transitions at elevated temperatures. This is in contrast to $KNbO_3$ which is a ferroelectric and undergoes several phase transitions at elevated temperatures. Even though $KNbO_3$ is paraelectric and cubic above 425 °C, the effects of thermal treatment in this material may be influenced by the domain structure and the possible remains of a local tetragonal distortion well above the phase transition, as in $BaTiO_3$ [13]. The comparison is also worth attention in order to provide an understanding of the end points of the solid solutions $KTa_{1-x}Nb_xO_3$ (KTN), which is a well known system allowing us to vary the macroscopic properties such as the ferroelectric behaviour.

In this paper we present results of x-ray diffraction, secondary ion mass spectrometry and atomic force microscopy which show that single crystals of $KTaO_3$ are indeed subject to a major reorganization of matter already at temperatures of 700 °C which leads to the formation of a chemically heterogeneous near-surface region with dramatic changes in the surface topography. Furthermore, our results indicate that the loss of K_2O has to be taken into account at temperature above 900 °C.

The single crystal of $KTaO_3$ used have been grown by the top-seeded solution-growth technique. Trace element analysis with spectrometrical methods showed that the level of impurities for the crystals was approximately 60 ppm. For x-ray diffraction analysis pieces of the same crystals were powdered to enhance the surface-to-bulk ratio. The size of the grains were of the order of 1.5 μm. The diffraction data were recorded by a Dron 1.5 diffractometer (Cu Kα) *in situ* at elevated temperatures. For surface analysis, (100)-oriented surfaces were obtained by mechanically polishing with an accuracy of $\pm 1^\circ$ or by cleaving. Both preparations allowed us to investigate surfaces which had a roughness of approximately 0.45 nm ($\pm$0.05) on 2×2 μm^2. Measurements by atomic force microscopy (AFM) were performed with an instrument by Nanoscope in air. It is important to note that the surface analysis was always carried out on new ('virgin') samples of the single crystalline material in order to avoid any influence of the specific thermal history. Similarly, pieces of the original single crystals were used for the thermogravimetrical measurements. Depth profiling by secondary ion mass spectrometry (SIMS) employed a Cameca 4f.

The x-ray diffraction data for oxidized $KTaO_3$ (700 °C) are presented in figure 1. The diffraction data for stoichiometric $KTaO_3$ exhibited only the standard lines typical for cubic perovskite (see table 1) and the lattice constant agreed well with the literature. In contrast, extra peaks are clearly discernible in the oxidized case as shown in figure 1 (compare with

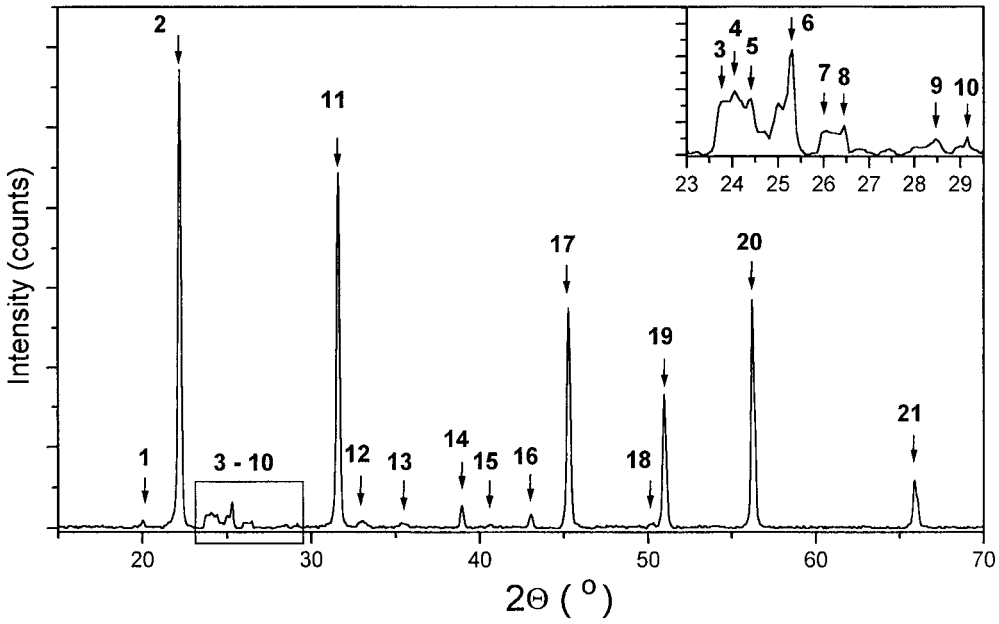

Figure 1. X-ray diffraction data (Cu Kα) for powdered single crystals of $KTaO_3$ at 700 °C at ambient conditions after several hours. Numbers indicated refer to table 1.

table 1). By analogy to other perovskites, especially $KNbO_3$ [12], it was tested whether these lines may originate from additional non-perovskite phases of character $KO^*(KTaO_3)_n$, the so-called Ruddlesden–Popper (RP) type phases [14]. For this, a simulation by the Rietveld method was performed assuming that $KTaO_3$ has a cubic structure with the dimension of the unit cell $= a$. The layer structure was then constructed with the bottom of a box having the dimensions $2a \times 2a$ and the height being approximated by $2n \times a +$ thickness of the unit cell of KO ($\widetilde{=}a$). The unit cell devised in this way consists of two stoichiometric units and has a symmetry corresponding to $I4/mmm$. In this case, the atomic positions of K are 0, 0, δ_{Z_K} and $\frac{1}{2}, \frac{1}{2}, \frac{1}{2} + \delta_{Z_K}$, of Ta: 0, 0, $\delta_{Z_{Ta}}$ and $\frac{1}{2}, \frac{1}{2}, \frac{1}{2} + \delta_{Z_{Ta}}$ and of O: 0, $\frac{1}{2}$, $\delta_{Z_{O1}}$; 0, $\frac{1}{2}$, $\frac{1}{2} + \delta_{Z_{O1}}$; $\frac{1}{2}$, 0, $\delta_{Z_{O1}}$; $\frac{1}{2}$, 0, $\frac{1}{2} + \delta_{Z_{O1}}$ for each O on the faces of the $KTaO_3$ unit cell and 0, 0, $\delta_{Z_{O2}}$; $\frac{1}{2}$, $\frac{1}{2}$, $\frac{1}{2} + \delta_{Z_{O2}}$ for O on the bottom of the $KTaO_3$ unit cell. The parameters δ_{Z_K}, $\delta_{Z_{Ta}}$, $\delta_{Z_{O1}}$ and $\delta_{Z_{O2}}$ are dependent on the multiplication factor according to the general formula $KO^*(KTaO_3)_n$. According to the simulation of scattering angles for various intercalation levels, here up to $n = 4$ (see table 1), the extra peaks do indeed coincide with angles originating from phases of the Ruddlesden–Popper (RP) type with $n = 2, 3$ and 4. Interestingly enough, these additional phases already formed after a relatively short time. Yet, the intensity varied appreciable with time with respect to the stoichiometric phase showing a maximum contribution of around 10% after 6–8 hours. This high dynamic prevented us from performing a complete Rietveld analysis of peak shape and intensity profile as the extra peaks changed within each measured spectrum (90–120 min). Finally notice that we did not observe any signature at these temperature related to metal-rich oxides in the diffraction pattern but instead identified some minor contributions from KO_2 (see table 1).

To provide further insights into the process occurring at elevated temperatures, thermogravimetrical measurements were conducted for a single crystal in the temperature range between 800 and 1000 °C. In figure 2 one can clearly see that some depletion of material

Table 1. Detailed analysis by Rietveld simulation of the x-ray diffraction data for $KTaO_3$ measured at 700 °C at ambient pressure as given in figure 1. Cell dimension of the pseudo-perovskite-structure ($Pm3m$): $a = 4.013$ Å (0.001). For the layer structure with symmetry $I4/mmm$ one obtains as cell dimension: $KO^*(KTaO_3)_2$: $A = B = a$, $C = 5a$; $KO^*(KTaO_3)_3$: $A = B = a$, $C = 7a$; $KO^*(KTaO_3)_4$: $A = B = a$, $C = 9a$.

No	d (Å)	2 theta (°)	I/I_0 (%)	Perovskite			$KO^*(KTaO_3)_2$			$KO^*(KTaO_3)_3$			$KO^*(KTaO_3)_4$		
1	4.436	20.01	1.7										0	0	8
2	4.006	22.19	100	1	0	0									
3	3.753	23.71	2.6										1	0	3
4	3.701	24.05	3.4							1	0	3			
5	3.648	24.4	3										0	0	10
6	3.522	25.29	5.7							0	0	8	1	0	5
7	3.431	25.97	1.3				1	0	3						
8	3.369	26.46	1.5				0	0	6						
9	3.134	28.48	0.8										1	0	7
10	3.064	29.14	0.9	$*KO_2*$											
11	2.832	31.59	77.4	1	1	0	1	1	0	1	1	0	1	1	0
							1	0	5	1	0	7	1	0	9
12	2.713	33.01	1.7				1	1	2				1	1	4
13	2.54	35.34	1.2										1	1	6
													1	0	11
14	2.314	38.92	5	1	1	1									
15	2.221	40.62	0.8							1	1	8	1	1	10
16	2.101	43.06	2.9	$*KO_2*$											
17	2.004	45.25	48.2	2	0	0	2	0	0	2	0	0	2	0	0
							0	0	10	0	0	14	0	0	18
18	1.813	50.31	1.2	?											
19	1.793	50.94	28.7	2	1	0									
20	1.637	56.19	49.2	2	1	1	2	1	5	2	1	7	2	1	9
							1	1	10	1	1	14	1	1	18
21	1.418	65.87	10.4	2	2	0									

$*KO_2*$ JCPDS card No 10-0235 (the two strongest lines).
Perovskite JCPDS card No 38-1470.

occurred for temperatures set at 800 and 900 °C, but that loss of material became substantial at around 1000 °C. Just like in $KNbO_3$, this is probably due to the easy volatilization of K_2O [10].

The results for (100) surfaces of $KTaO_3$ with atomic force microscopy are summarized in figures 3–5. Shown are typical examples for surfaces without (figure 3) and with heat-treatment (figures 4 and 5) for the cleaved as well as the mechanically polished samples. The various AFM results included exemplify the variety of topographical rearrangement possible for the cleaved (compare figures 4(a) and 4(c)) and the polished samples (compare figures 5(a) and 5(b)), respectively. We found these trends to be typical of the kind of surface under consideration both for the different crystals available to us as well as separate pieces of the same crystal. The comparison with the surface prior to thermal treatment revealed a dramatic redistribution of matter due to the annealing process. After oxidation the cleaved surface showed the occurrence of large terraces with a parallel alignment (figure 4(a)). This alignment seems to originate from an underlying structure already present on the surface prior to heat-treatment as indicated in figure 3(a). The top of the terraces shows large regions covered predominantly with nano-crystalline features (step-terrace like) of height typically 6 Å ± 0.2 and 12 Å ± 0.2 (see figure 4(b)), but also in a few cases 4 Å (step height characteristic of

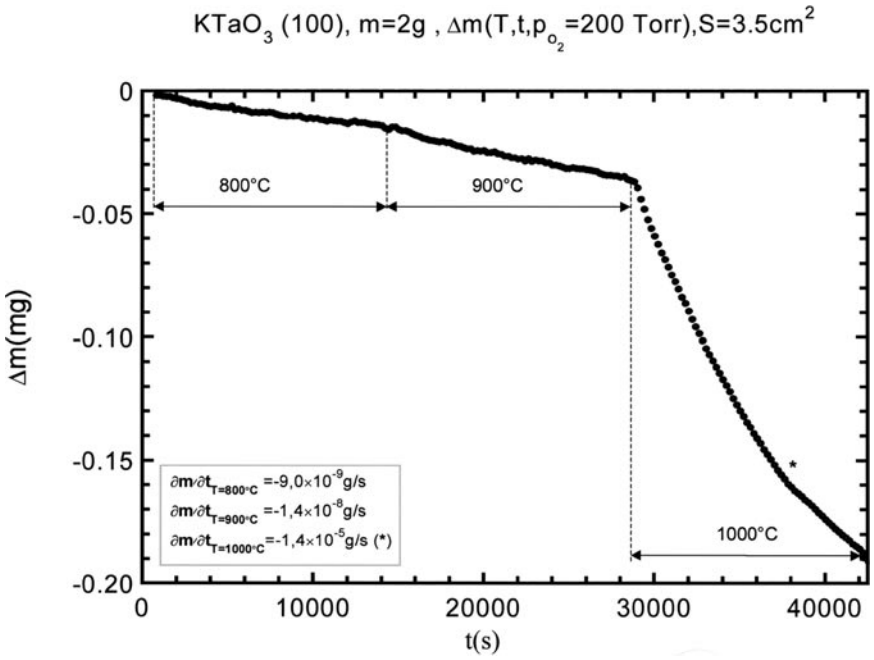

Figure 2. Thermogravimetrical measurements of a single crystalline $KTaO_3$ at elevated temperatures.

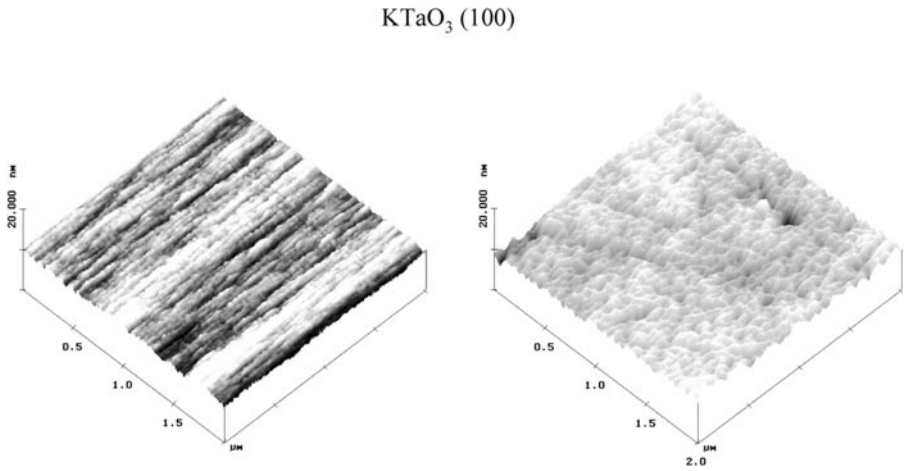

Figure 3. Atomic force microscopy for (100) surfaces of $KTaO_3$ prior to heat-treatment. Figure 3(a) shows the pseudo-3D image of a surface after cleavage, whereas figure 3(b) provides the corresponding image for a mechanically polished surface.

the original surface) as well as 20 Å. This kind of topographical reorganization of the surface seems to be characteristic of a layer growth, here perpendicular to the (100) surface. In the given example in figure 4(b), the dimension of the area with these nano-steps is of the order 400×400 nm^2, but may easily extend to μm^2 at other places. At other segments of the cleaved surface, which probably deviate from the ideal (100) orientation, these features are

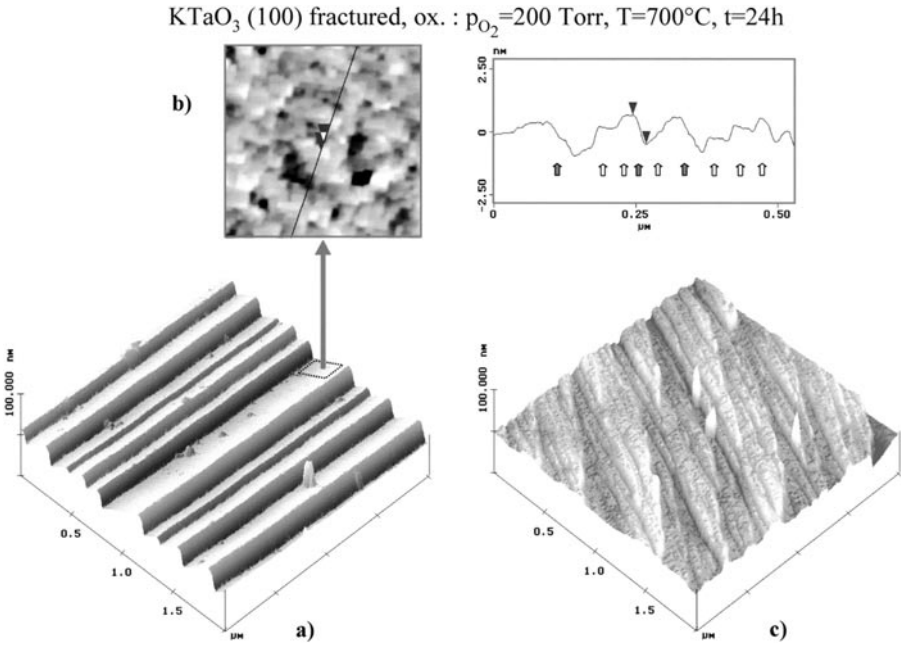

Figure 4. Atomic force microscopy of cleaved (100) surfaces after heat treatment at 700 °C at ambient conditions. Shown are the pseudo-3D presentation for the kid of topography found on cleaved surfaces (a), (c). A 'flat' segment on top of the terrace is enlarged (b) with a line scan indicating a step-height of predominantly 6 Å (open arrow) or 12 Å (shaded arrow).

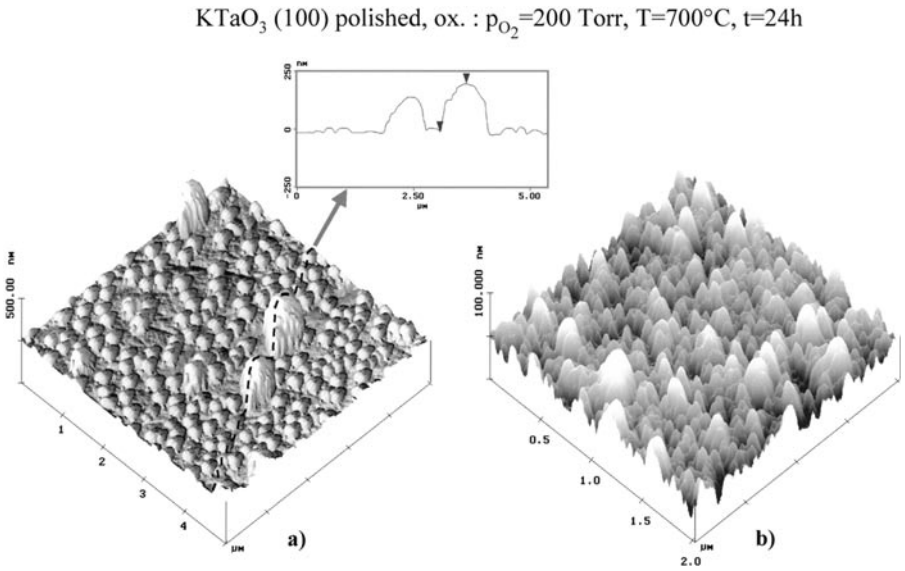

Figure 5. Atomic force microscopy of polished (100) surfaces after heat treatment at 700 °C at ambient conditions. Shown are the pseudo-3D presentations for different locations on the surfaces (a), (b). Crystals grown on top of the surface may be as high as 200 nm (indicated by arrows) for the kind of preparation conditions employed as visualized by a line scan (inset).

not as clearly discernible. In fact, figure 4(c) highlights the kind of complex topographical modification also observable on these kinds of surface.

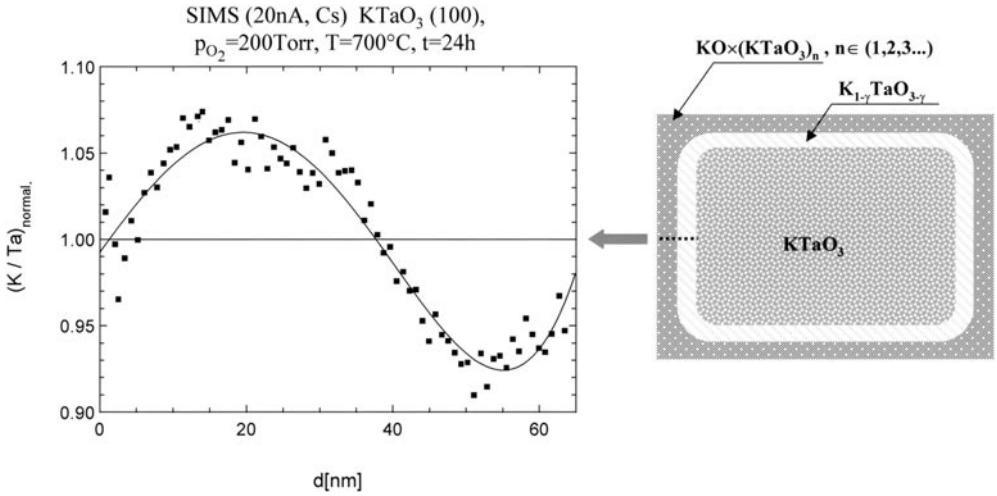

Figure 6. Schematic visualization of the chemical heterogeneity in the near-surface region and a typical depth-profile of the relative distribution of K compared to Ta after heat-treatment as obtained by secondary ion mass spectrometry. Shown are the relative ratios of K/Ta after normalizing each profile with respect to depth profiles measured with the same experimental settings of the instrument for a sample of $KTaO_3$ without heat-treatment. The solid line is only introduced to highlight the trends in the K/Ta ratio. The general form of the measured relative distribution is characteristic for the kind of heat-treatment employed though the exact numbers have been found to vary between different locations on the surface. Close to the surface the details of the profile have to be taken with caution as the sputter equilibrium is not immediately reached and different samples are employed.

The mechanically polished samples gave yet another picture of the morphological changes of the surface after heat-treatment. Two main types of topography may be distinguished: the appearance of an irregular distribution of new crystals (figure 5(a)), some of which may be as high as 0.2 μm for the given experimental conditions, and, on the other hand, portions of the surface which become completely covered by nano-crystallites with a maximum height of 80–100 nm for the heat-treatment employed (see figure 5(b)). The kind of modification on the polished surfaces did not allow us to find large enough flat regions to detect unambiguously the formation of the steplike nano-crystals which were discovered on the cleaved surfaces.

Combining these experimental observations establishes clearly that the equilibration processes at elevated temperatures cannot be simply described by standard point defect models. Instead, new chemical phases form at 700 °C with, in addition, a massive modification of the surface morphology. The existence of the non-perovskite phases in $KTaO_3$ did not come as a total surprise as they had already been observed for $KNbO_3$ ([12], see also [15]). But notice, in the case of $KNbO_3$ this phenomenon occurred at much lower temperatures (500 °C). The formation of the new kind of phases is due to an intercalation of KO which causes the symmetry of the crystal structure to change from $Pm3m$ to $I4/mmm$. Since the thermogravimetrical measurements did not provide evidence of an appreciable uptake or substantial loss of material, the growth of these new phases must almost exclusively be caused by a redistribution of material within the crystals. This becomes evident from inspection of SIMS depth profiles. As can be taken from figure 6, the oxidation process leads to an enrichment of K with respect to Ta close to the surface and a corresponding depletion in deeper parts of the crystal. As in $KNbO_3$ ([12], compare also with $SrTiO_3$ [16, 17]) this seems to result from a segregation of K towards the surface for the experimental conditions applied. The depth profiles do not contain chemical information but only elemental distribution. Yet, combining the results of the x-ray

diffraction data with the concentration profiles we can conclude that the redistribution of K (most probably in form of KO) leads to the formation of the KO-enriched RP phases close to the surface and a corresponding KO-deficiency in deeper parts of the near-surface region. The resulting 'skin' region of the crystal with its multilayer-type arrangement is schematically summarized in figure 6(b) and extends for the kind of preparation conditions employed at least up to 60–70 nm.

So far, the standard description of the defect chemistry of $KTaO_3$ relied solely on the existence of oxygen vacancies [7]. At the heart of this description lies the defect chemistry diagram obtained by variation of temperature and partial pressure of oxygen and measurement of the so-called equilibrium electrical conductivity. Yet, it is already known from thermodynamical arguments that a third component is necessary to define the chemical composition [18]. The activity of the volatile AO component has been identified as a possible candidate [19, 20] and has been introduced into defect chemistry as γ-nonstoichiometry ($A_{1-\gamma}BO_{3-\gamma}$). This scheme has been discussed in terms of a bulk nonstoichiometry for a PbO-depleted $PbZrO_3$ [19] and a local nonstoichiometry in the case of $BaTiO_3$ [20]. Applying these ideas to $KTaO_3$, the low temperature regime (up to 800–900 °C) is similar to the situation encountered in $SrTiO_3$ [15, 16], $BaTiO_3$ [21] and $KNbO_3$ [12, 15]. The inhomogeneity develops in these materials at elevated temperatures due to the redistribution of AO near the surface with subsequent solid state reactions leading to AO-rich and AO-depleted phases. In this picture, the surplus of KO on and close to the surface of $KTaO_3$ can then be regarded as a surface segregation for a local γ-nonstoichiometry ($K_{1-\gamma}TaO_{3-\gamma}$), which, in turn, leads to the observed RP phases $KO^*(KTaO_3)_n$. It is most likely that the processes involved have to be described, as in case of $KNbO_3$ [12], by a dismantling and intercalation of KO layers. The relatively low temperatures at which these effects take place make it necessary to take into account the existence of fast transport paths such as extended defects [12]. Notice in this context that occurrence of an unusually high density of extended defects close to the surface has recently been experimentally verified in case of $SrTiO_3$ [22]. Possible driving forces leading to the kind of chemical rearrangement at and near the surface of $KTaO_3$ may be taken from the extensive discussion for $SrTiO_3$ in [17].

These processes must necessarily lead to changes in the morphology of the surface. We therefore interpret the dramatic effects observed by the AFM to the outlined restructuring with the formation of new crystalline features. The differences as evident from figures 4 and 5 may then be related to the character and quality of the surface. We take the massive terrace-like reorganization in figure 4(a) as a signature of the underlying defect structure of the crystal which allows us to transport material easily towards the surface via extended defects. The formation of the nano-crystalline features discovered on top of the terraces (see again figure 4(b)) seem to proceed uniformly perpendicular to the surface, in this case an almost ideal planar (100) surface. It is tempting to consider the intercalation of KO into the perovskite lattice to be situated parallel to the surface (in correspondence with the already mentioned layer growth). In this context, we would like to draw attention to the correlation in step-height of the nanocrystalline structures with the lattice constant of an RP phase with $n = 1$ (12.1 Å) or half the size of its unit cell (6 Å). Note also the large similarity in form with the topographical changes encountered in $SrTiO_3$ [17]. The redistribution of KO and structural accommodation as in the case of figure 4(c) may be quite different as a consequence of the deviation from the ideal (100) orientation.

Similarly, the morphology of the polished surface is obviously subject to an immense rearrangement. Yet, the polished surfaces did not show the same kind of reorganization of the surface as the cleaved surface, though the original surfaces in both cases exhibited a similar roughness on the microscopic scale. Several reasons may give rise to the difference in behaviour

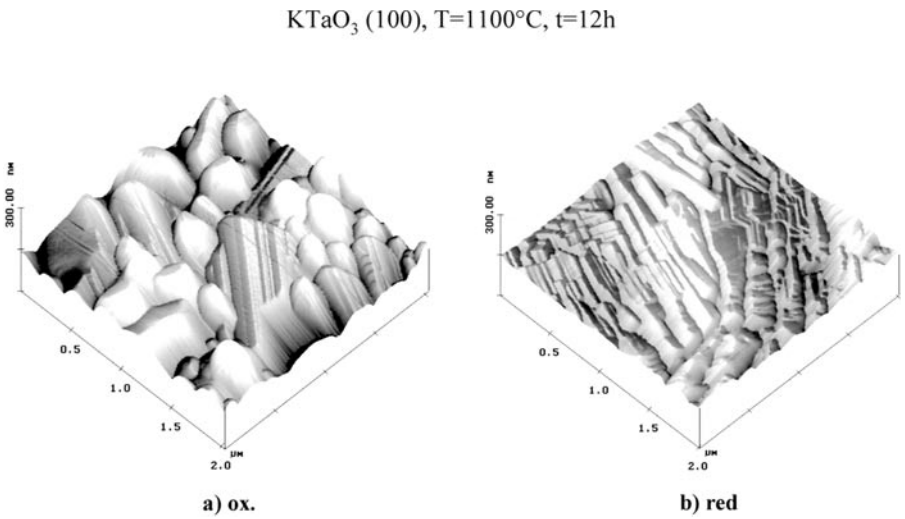

Figure 7. Atomic force microscopy of polished (100) surfaces after heat-treatment at 1100 °C for oxidizing (a) and reducing (ultra-high vacuum) conditions (b).

of the polished in comparison to the cleaved surfaces. The orientation of our surfaces may not be as perfect as for the cleaved surface. Or, one may have to take into consideration an influence of the chemical treatment during polishing. For instance, we cannot exclude the possibility of element-specific leaching processes in aqueous solution, in particular along the extended defects. Also, the formation of dislocations may be significantly different by polishing compared to cleaving. At the same time note that the resulting character of the surfaces after heat-treatment seems to depend critically on the underlying structure of each surface prior to heat-treatment which is distinctly different for both kinds of surface (compare, e.g., figure 5(b) with figure 3(b) for the polished and figure 4(a) with figure 3(a) for the cleaved surface).

The presented experimental results focus on temperatures below 800 °C. As already mentioned above, for temperatures above 900–1000 °C the additional loss of alkali ions sets in, leading to KO-deficient $KTaO_3$ (γ-nonstoichiometry). In fact, we detected lines originating form TaO_x in x-ray diffraction data for $KTaO_3$ crystals prepared at about 1000 °C. Consequently, proper experiments above 900 °C should be conducted in an atmosphere rich in potassium oxide. We have not performed such experiments. Instead, we only want in the present paper to provide an experimental illustration of the kind of effect to be expected for surfaces of $KTaO_3$ subjected to a heat-treatment characteristic for the developing K deficiency. The corresponding AFM measurements for crystals exposed to such temperature (here 1100 °C) reveal indeed a further dramatic increase in the topographical rearrangement of the surface (see figure 7(a)). In addition, we inspected the surface modifications which result from a high-temperature treatment under vacuum conditions. As may be taken from figure 7(b), the impact on the surface morphology is as massive as for oxidizing conditions, though clearly different in character. The applied conditions correspond to the so-called p- and n-type regime of electrical conductivity, respectively, as investigated by Deputy and Vest [7]. Their electrical characterization covered the high-temperature regime between 900 and 1300 °C, but did not control the K_2O vapour pressure. Yet, their model of point defect chemistry relied on the assumption of a constant K:Ta. The experimental evidence suggest that this is clearly violated. Our data give further support to the caution expressed by Raevski *et al* [11] to consider both

oxygen as well as alkali metal loss when characterizing the electrical properties of reduced $KTaO_3$ above 800 °C.

In conclusion, our results for single crystals of $KTaO_3$ prepared under oxidizing conditions at elevated temperatures (below the demarcation line of KO depletion) demonstrate the existence of Ruddlesden–Popper type phases, $KO^*(KTaO_3)_n$, a redistribution of potassium with respect to tantalum within the near-surface region and corresponding dramatic changes of the topography of (100) surfaces. The results are interpreted in terms of the development of a chemically heterogeneous near-surface region for oxidizing conditions, which results from an interplay of segregation processes within the crystal and the intergrowth of KO. Atomic force microscopy reveals complex modifications of the surface morphology at elevated temperatures. In particular, the formation of step-terrace-like nano-crystallites with step heights of 6 Å and 12 Å can be observed. Comparison of surfaces obtained by cleavage and polishing indicate that changes on the surface depend also critically on sample preparation. Further studies are necessary to analyse the details of the evolving distribution of non-perovskite phases on the surface and within the near-surface region as well as the underlying driving forces.

For temperatures above 900–1000 °C, the additional effect of an evaporation of K_2O comes into play. The corresponding morphological reorganization of the surface at 1100 °C under both oxidizing and reducing (UHV) conditions were recorded by atomic force microscopy.

These observations are in strong contrast to the standard concept of defect chemistry for $KTaO_3$ which considers only the statistical distribution of point defects in an otherwise homogeneous medium. The possibility of a restructuring within the near-surface region with the formation of new chemical phases necessitates a new description for heat-treated perovskite containing potassium. In particular, the results indicate that the preparation conditions applied in a standard manner (even below temperatures of developing KO deficiency) do not produce equilibrated crystals, but instead lead to a chemically heterogeneous near-surface region which continuously changes in time at elevated temperatures. Furthermore, the observed new phases of Ruddlesden–Popper type have not been reported before, which also implies that the pseudo-binary phase diagram of K_2CO_3–Ta_2O_5 may need revision.

Acknowledgments

We would like to acknowledge the expert help of Ch Freiburg and W Reichert from the central analytical department of the research center in Jülich, who provided x-ray analysis for comparison from stoichiometric reference samples as well as from crystals heated above 900 °C. We would also like to thank H Holzbrecher from the same department for his contribution to the microanalysis by SIMS.

References

[1] Mattheis L F 1972 *Phys. Rev.* B **6** 4718
Xu Y-N, Ching W Y and French R H 1990 *Ferroelectrics* **111** 23
Neumann T, Borstel G, Scharfschwerdt C and Neumann M 1992 *Phys. Rev.* B **46** 10 623
Postnikov A V, Neumann T, Borstel G and Methfessel M 1993 *Phys. Rev.* B **48** 5910
[2] Grass M, Braun J, Postnikov A, Borstel G, Ünlü H and Neumann M 1996 *Surf. Sci.* **352–354** 760
Krasovskii E E, Krasovska O V and Schattke W 1997 *J. Electron Spectrosc. Relat. Phenom.* **83** 121
[3] Singh D J 1996 *Phys. Rev.* B **53** 176
[4] Gutmann R, Hulliger J and Reusser E 1993 *J. Cryst. Growth* **126** 578
Kwak B S, Erbil A, Budai J D, Chisholm M F, Boatner L A and Eilkens J F 1994 *Phys. Rev.* B **49** 14 865
[5] Prusseit W, Boatner L A and Rytz D 1993 *Appl. Phys. Lett.* **63** 3376
Feenstra R, Boatner A, Budai L D, Christen D K, Galloway M D and Poker D B 1989 *Appl. Phys. Lett.* **54** 1068

[6] Höchli U T, Knorr K and Loidl A 1990 *Adv. Phys.* **39** 405
Vugmeishter B E and Glinchuk M D 1990 *Rev. Mod. Phys.* **62** 993
[7] Deputy G O and Vest R W 1978 *J. Am. Ceram. Soc.* **61** 321
[8] Exner M, Donnerberg H, Catlow C R A and Schirmer O F 1995 *Phys. Rev.* B **52** 3930
[9] Donnerberg H 1999 *Springer Tracts in Modern Physics 151* (Berlin: Springer)
[10] Flückiger U and Arend H 1978 *J. Cryst. Growth* **43** 406
[11] Raevski I P, Maksimov S M, Fisenko A V, Prosandeyev S A, Osipenko I A and Tarasenko P F 1998 *J. Phys.: Condens. Matter* **10** 8015
[12] Szot K, Speier W, Cramm S, Herion J, Freiburg Ch, Waser R, Pawelczyk M and Eberhardt W 1996 *J. Phys. Chem. Solids* **57** 1765
[13] Anlikier M, Brugger H R and Känzig W 1954 *Helv. Phys. Acta* **27** 99
[14] Ruddlesden S N and Popper P 1957 *Acta Crystallogr.* **10** 538
Ruddlesden S N and Popper P 1958 *Acta Crystallogr.* **11** 54
See also Drys M and Trzebiatowski W 1957 *Roczniki Chem.* **31** 489
Lukaszewicz K 1958 *Angew. Chem.* **70** 320
Lukaszewicz K 1959 *Roczniki Chem.* **33** 239
[15] Szot K, Pawelczyk M, Herion J, Freiburg Ch, Albers J, Waser R, Hulliger J, Kwapulinski J and Dec J 1996 *Appl. Phys.* A **62** 335
[16] Szot K, Speier W, Herion J and Freiburg Ch 1997 *Appl. Phys.* A **64** 55
[17] Szot K and Speier W 1999 *Phys. Rev.* B **60** 5909
[18] Nowotny J and Rekas M 1991 *Solid State Ion.* **49** 135
[19] Prisedskii V V, Komarov V P, Pan'ko G F and Kilmov V V 1980 *Ferroelectrics* **23** 23
[20] Prisedskii V V and Tret'yakov Y D 1982 *News Acad. Sci. USSR Inorg. Mater.* **18** 1926
[21] Szot K, Freiburg Ch and Pawelczyk M 1991 *Appl. Phys.* A **53** 563
[22] Wang R, Zhu Y and Shapiro S M 1998 *Phys. Rev. Lett.* **80** 2370